sample, 81525 $\pm$ 385 (stat) for $W^+ \to e^+\nu$ sample and 54356 $\pm$ 315 (stat) for $W^- \to e^-\overline{\nu}$ sample, with negligible correlation. The ratio of the inclusive, $W^+ \to e^+\nu$ and $W^- \to e^-\overline{\nu}$ yields between this method and the parameterized QCD shape is 0.998 $\pm$ 0.007, 0.999 $\pm$ 0.007 and 0.993 $\pm$ 0.007 respectively, considering only the uncorrelated systematics between the two methods.

9.4 $W \to \mu\nu$ QCD Background Modeling and Signal Extraction

We use fixed shape templates for the signal and backgrounds.

The $\not{E}_T$ shape of the QCD background component is obtained from a high purity QCD sample selected following the same selection as for the signal, except for the isolation cut. Events with a not-isolated muon, having $I^{\text{rel}}_{\text{comb}} > 0.2$ (as shown in Figure **??**) are kept.

Simulation studies indicate that this template does not fully reproduce the $\not{E}_T$ shape of the isolated region. This is shown in Figure 12 (left), where the solid line represents the template from the isolated region and the dashed line the template obtained inverting the isolation requirement.

A positive correlation between the isolation variable, $I^{\text{rel}}_{\text{comb}}$, and $\not{E}_T$ (Figure 12, right) can be appreciated. This behaviour can be parametrized in terms of a linear function $\not{E}_T \propto (1 + \alpha\, I^{\text{rel}}_{\text{comb}})$, as it is shown in the same Figure. The correlation is subsequently removed applying a correction of the kind $\not{E}'_T = \not{E}_T/(1 + \alpha\, I^{\text{rel}}_{\text{comb}})$, to the events in the not-isolated region and a new, corrected template, is obtained. The agreement of this new template (solid dots in Figure 12, left) with the prediction from the isolated region is considerably improved. It is also observed that a maximal variation in the correcting factor of $\Delta\alpha = \pm 0.08$ successfully covers the MC truth prediction for the isolated region over the whole $\not{E}_T$ interval (shaded area in the Figure).

The same behaviour is observed in the data, a positive correlation between $\not{E}_T$ and $I^{\text{rel}}_{\text{comb}}$ (open circles in Figure 12, right). We calculate and apply a correction $\not{E}'_T = \not{E}_T/(1 + \alpha\, I^{\text{rel}}_{\text{comb}})$, with $\alpha \approx 0.2$. The templates obtained in data are shown in Figure 13; the uncorrected and corrected data template from the not-isolated region, together with the MC expectation for the isolated one, are given. The shaded area in the Figure is bounded by two templates, obtained using two extreme correction parameters $\alpha \pm \Delta\alpha$, with $\Delta\alpha = \pm 0.08$, as evaluated by MC. This area is taken to be the systematic uncertainty in the QCD background shape.

Several parameterizations for the correction have been tried but the impact on the corrected template and therefore on the final result is small. Associated uncertainties in the cross section and ratio are evaluated as the differences between fitted values using the optimal α value to derive the corrected template and the two extreme cases $\alpha \pm \Delta\alpha$.

The following signal yields are obtained: 140757 $\pm$ 383 for the inclusive sample, 56666 $\pm$ 240 for $W^- \to \mu^-\overline{\nu}$ sample and 84091 $\pm$ 291 for $W^+ \to \mu^+\nu$ sample.

The fitted $\not{E}_T$ distributions are presented in Figure 14 (full sample) and Figure 15 (samples separated by muon charge). The fitted individual contributions of the W signal, EWK processes and QCD are also shown in the plots. Figures 14 and 15 show the $\not{E}_T$ distributions for data and fitted signal plus background components. Figures 16 and 17 show the M_T distributions for data and fitted signal plus background components.

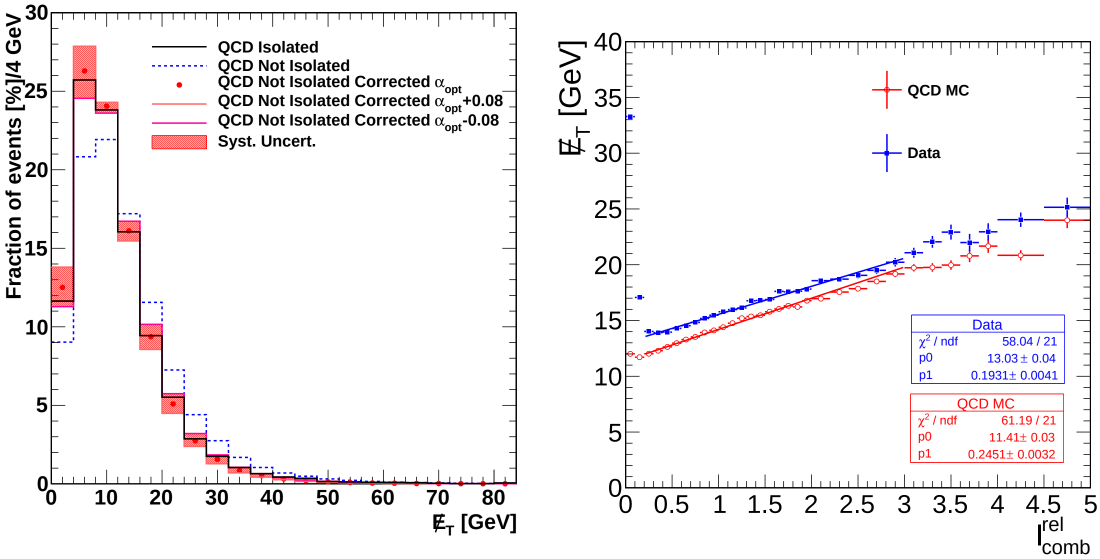

Figure 12: Left: MC expectation for the $\not\!\!E_{\mathrm{T}}$ shape of QCD events with isolated muons (solid histogram), for the $\not\!\!E_{\mathrm{T}}$ template obtained from the not-isolated sample (dashed histogram) and for the isolation-corrected template (black points). The shaded area, subtended by the templates corrected with factors $\alpha \pm \Delta\alpha$, with $\Delta\alpha = \pm 0.08$, covers the prediction for the isolated region over the full $\not\!\!E_{\mathrm{T}}$ region. Right: Distribution of $\not\!\!E_{\mathrm{T}}$ versus the isolation quantity. Open circles are the MC expectation for QCD events and filled squares are the data distribution. The high values of $\not\!\!E_{\mathrm{T}}$ in the first two bins in the isolation variable are due to the presence of the W signal events. The lines are linear function fits in the range [0.2, 3.] in the Isolation variable.

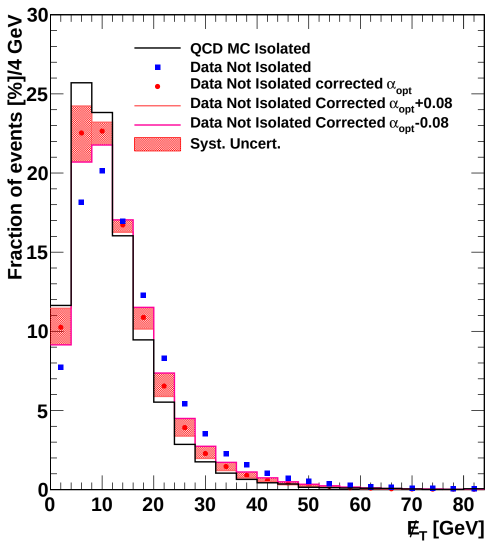

Figure 13: Corrected $\not\!\!E_{\mathrm{T}}$ QCD template obtained from the non-isolated events ($I^{\mathrm{rel}}_{\mathrm{comb}} > 0.2$) of the preselected data sample (filled dots). It is compared with the template from plain inversion on the isolation variable (filled squares) and with the QCD MC expectation for the isolated region $I^{\mathrm{rel}}_{\mathrm{comb}} < 0.1$ (solid black histogram). The shaded area is limited by two templates, obtained using correction parameters $\alpha \pm \Delta\alpha$ with $\Delta\alpha = \pm 0.08$ (see text).

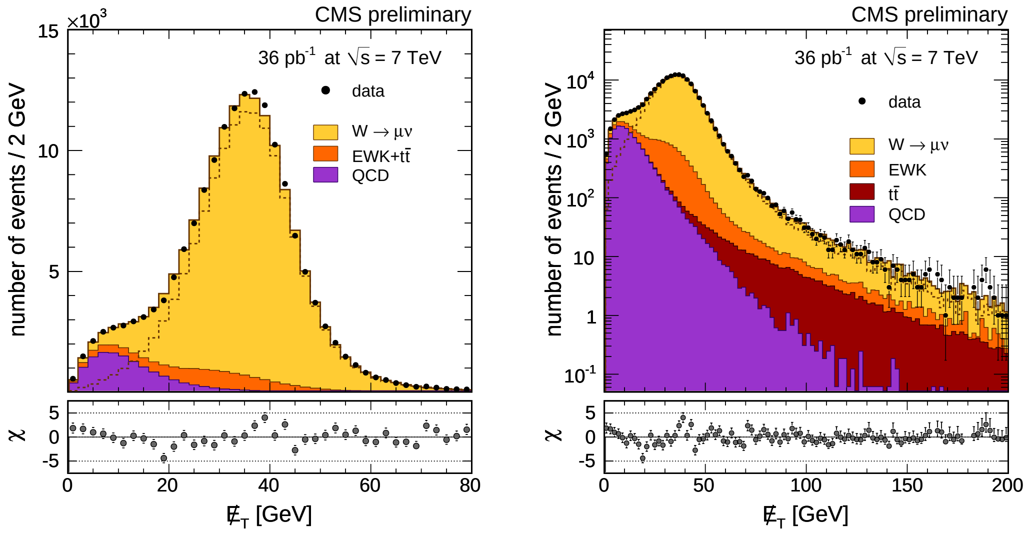

Figure 14: Total $\not\!\!E_{\mathrm{T}}$ spectrum (black dots) and fitted contributions from the different processes shown stacked, W signal (light yellow histogram), other EWK processes (medium orange histogram), and QCD background (dark purple histogram).

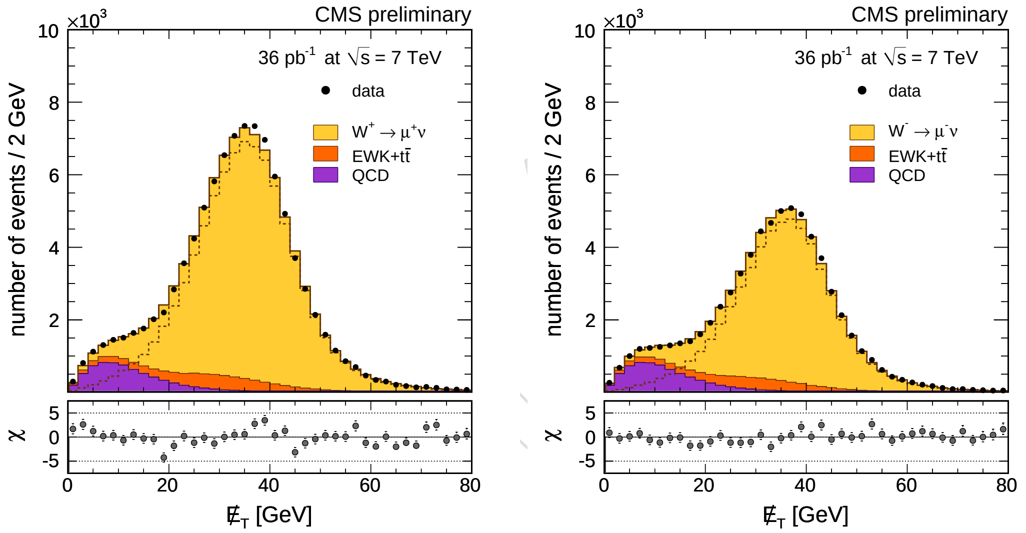

Figure 15: W^+ (left) and W^- (right) experimental distributions (black dots), together with the fitted contributions from the different processes (shown stacked): W signal (light yellow histogram), other EWK processes (medium orange histogram), and QCD background (dark purple histogram).

10 $\mathrm{Z} \longrightarrow \ell^+\ell^-$ Signal Extraction

The inclusive $\mathrm{Z} \to \ell^+\ell^-$ yield can be obtained counting the number of selected candidates after subtracting the residual background, correcting for the estimated lepton selection efficiencies. We also fit the $\mathrm{Z} \to \ell^+\ell^-$ yield and lepton efficiencies using a simultaneous fit to the invariant mass spectra of multiple di-lepton categories. The simultaneous fit deals correctly with correlations in determining the lepton efficiencies and the Z yield from the same sample. The Z yield extracted in this way does not need to be corrected by efficiency effects in order to determine the cross section, and the statistical error on the Z yield absorbs errors on the determination of electron efficiencies that would be propagated as systematic uncertainties in the counting anal-